CONTROLLING PICOLITRE DROPLET IMPACT DYNAMICS BY TAILORING THE SOLID SUBSURFACE

P. S. Brown[a], E. L. Talbot[a], T. J. Wood[a], M. J. Egan[a], J. J. Wu[b], K. Saini[c], N. Kumar[c], C. D. Bain[a], and J. P. S. Badyal[a]*

[a] Department of Chemistry, Durham University, Durham DH1 3LE, England, UK

[b] School of Engineering and Computing Sciences, Durham University, Durham DH1 3LE, England, UK

[c] School of Mechanical, Materials, and Energy Engineering, Indian Institute of Technology Ropar, Punjab 140001, India

* Corresponding author email: j.p.badyal@durham.ac.uk

HIGHLIGHTS

• Oscillatory dynamics of picolitre water droplet impact onto solid surfaces.

• Influence of surface functionality.

• Role of underlayer stiffness and thickness.

• Softer and thicker films display higher oscillation frequencies.

GRAPHICAL ABSTRACT

Impact   Oscillation
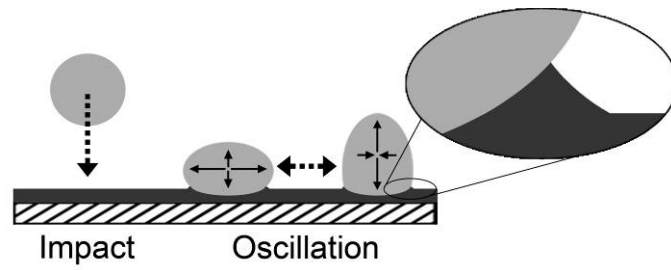
ABSTRACT

The oscillatory dynamics of picolitre water droplets following impact onto a range of hydrophobic surfaces is found to be influenced by the underlayer stiffness and thickness. The relative contributions of surface functionality versus subsurface hardness have been decoupled by utilising plasmachemical surface functionalisation and underlayer crosslinking respectively. Higher oscillation frequencies are measured for softer and thicker films, which correlates to a larger surface deformation around the liquid droplet contact line.

1. INTRODUCTION

The impact of liquid droplets onto soft surfaces is an important phenomenon underpinning a plethora of industrial processes including microfluidics,[1,2] electrowetting,[3] droplet condensation,[4] and inkjet printing (applications in microelectronics,[5,6,7,8] pharmaceutical dosing or screening,[9,10,11] tissue engineering,[12,13] and optics[14,15]).

Previous studies have shown that the vertical component of the surface tension resulting from a liquid droplet resting on a soft surface can induce the formation of a wetting ridge, Figure 1, where the surface along the droplet contact line deforms.[16,17,18,19,20,21] These deformations can perturb the dynamics of droplet spreading[22] (viscoelastic braking) and have been seen to enhance contact line pinning in microlitre droplets.[23]
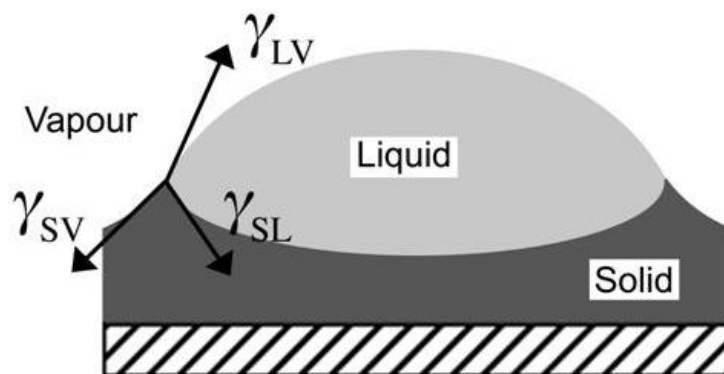

Figure 1: Schematic diagram showing a wetting ridge formed on a soft surface due to the vertical component of the liquid-vapour surface tension, γ_{LV}.

A comparison of the oscillation of microlitre droplets following impact onto hard and soft surfaces has shown that droplets oscillate at a higher frequency on the latter.[24] This has been explained in terms of the deformed wetting ridge enhancing droplet pinning and reducing the amount of energy dissipation through contact line motion. However, the dependency of such behaviour upon the subsurface properties has not previously been investigated.

In this article, the impact dynamics of picolitre water droplets onto a range of different thickness films with controllable hardness and surface wettability has been studied, Figure 2. Firstly, non-crosslinked and crosslinked plasma fluorinated polybutadiene films have been compared whilst maintaining the same hydrophobic surface chemistry.[25] An alternative system comprises surface initiated atom transfer

radical polymerisation (ATRP)[26] growth of hydrophobic perfluorinated acrylate brushes with well-defined polymer chain length,[27] where plasma chlorinated polybutadiene is utilised as an ATRP initiator layer.
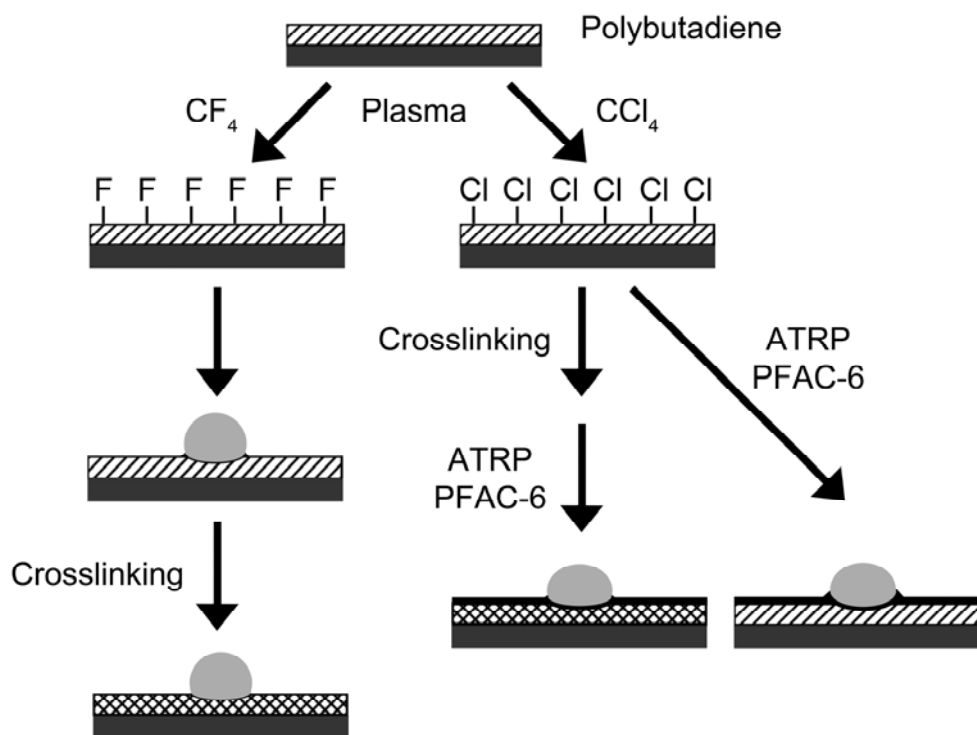

Figure 2: Summary of functional surfaces investigated for water droplet impact onto spin coated polybutadiene followed by variants of plasmachemical halogenation, crosslinking and growth of ATRP polymer brushes. PFAC-6 denotes 1H,1H,2H,2H-perfluorooctyl acrylate monomer for ATRP.

2. EXPERIMENTAL

2.1 Variable Thickness and Hardness Plasma Halogenated Polybutadiene Films

Polished silicon (100) wafers (Silicon Valley Microelectronics, Inc.) were used as substrates. Polybutadiene (M_w = 420,000, 36% cis 1,4 addition, 55% trans 1,4 addition, 9% 1,2 addition, Sigma-Aldrich Inc.) dissolved in toluene (+99.5%, BDH) at various concentrations was spin coated using a photoresist spinner (Cammax Precima) operating at 3000 rpm. Any trapped solvent within these polymer films was then removed by annealing under vacuum at 90 °C for 60 min.

Plasmachemical fluorination (or chlorination for surface initiated ATRP) of the

polybutadiene films was undertaken in a cylindrical glass chamber (5 cm diameter, 470 cm^3 volume) connected to a two stage rotary pump via a liquid nitrogen cold trap (2 x 10^{-3} mbar base pressure and a leak rate better than 6 x 10^{-9} mol s^{-1}) and enclosed in a Faraday cage. An L-C matching unit was used to maximise power transmission between a 13.56 MHz radio frequency generator and a copper coil externally wound around the glass reactor. Prior to each plasma treatment, the chamber was scrubbed with detergent, rinsed in propan-2-ol, and further cleaned using a 50 W air plasma for 30 min. Next, a piece of polybutadiene coated substrate was placed into the reactor (8 cm downstream to avoid surface texturing[28,29,30]), followed by evacuation to base pressure. CF$_4$ gas (+99.7%, Air Products) (or CCl$_4$ vapour (99.5%, May & Baker Ltd.)) was then admitted into the system via a needle valve at a pressure of 0.2 mbar and 2 cm^3 min^{-1} flow rate, and the electrical discharge ignited using a power of 50 W for 60 s. Upon completion of surface functionalization, the gas (vapour) feed was switched off and the chamber vented to atmosphere. Subsequent crosslinking of these plasma fluorinated (chlorinated) polybutadiene films entailed placing them in a vacuum oven at 155 °C for 60 min.[25]

2.3 Surface Initiated Atom Transfer Radical Polymerisation (ATRP)

The plasma chlorinated polybutadiene initiator coated silicon wafer pieces were loaded inside a sealable glass tube containing copper(I) bromide (5 mmol, 98%, Sigma Aldrich Ltd.), copper(II) bromide (0.01 mmol, 99%, Sigma Aldrich Ltd.), 2-2'-bipyridyl (10 mmol, ≥98%, Sigma Aldrich Ltd.), trifluorotoluene (4 mL, >99%, Sigma Aldrich Ltd.), and 1H,1H,2H,2H-perfluorooctyl acrylate (0.05 mol, 95%, Fluorochem Ltd.).[27] The mixture was thoroughly degassed using several freeze-pump-thaw cycles and then the sample tube immersed into an oil bath maintained at 95 ºC for 16 h to allow polymerisation to take place. Finally, the cleaning and removal of any physisorbed polymer was undertaken by Soxhlet extraction with hot toluene for 5 h.

2.4 Surface Characterisation

A VG ESCALAB spectrometer equipped with an unmonochromatised Mg K$_\alpha$ X-ray source (1253.6 eV) and a concentric hemispherical analyser (CAE mode pass energy = 20 eV) was used for X-ray photoelectron spectroscopy (XPS) analysis. Core level XPS spectra were fitted to a linear background and equal full-width-at-half maximum (FWHM) Gaussian components and referenced to the C(1s) -$\underline{C}_xH_y$

hydrocarbon peak at 285.0 eV.[31] Surface elemental compositions were calculated using sensitivity factors derived from chemical standards, C(1s): O(1s): F(1s): Cl(2p): Si(2p) equals 1.00: 0.36: 0.24: 0.39: 0.96.

Fourier transform infrared (FTIR) analysis of the deposited layers was undertaken using an FTIR spectrometer (Spectrum One, Perkin-Elmer Inc.) equipped with a liquid nitrogen cooled MCT detector. Spectra were recorded at a resolution of 4 cm^{-1} across the 700–4000 cm^{-1} wavelength range. Reflection absorption infrared spectroscopy (RAIRS) measurements were performed using a variable angle accessory (Specac Ltd.) set at 66° and fitted with a KRS-5 polarizer to remove the s-polarized component.

Thickness measurements of films deposited onto silicon wafers were made using a spectrophotometer (nkd-6000, Aquila Instruments Ltd). The obtained transmittance-reflectance curves (350–1000 nm wavelength range) were fitted to a Cauchy model for dielectric materials using a modified Levenberg-Marquardt algorithm.[32]

Microlitre sessile drop contact angle analysis was carried out with a video capture system (VCA2500XE, AST Products Inc.) using 1.0 µL dispensation of de-ionised water. Picolitre drop impact studies were carried out using a piezo-type nozzle (MicroFab MJ-ABP-01, Horizon Instruments Ltd.) with an aperture diameter of 30 µm. Water drops of 30 µm diameter (14 pL volume) were generated by applying a drive voltage of 30 V and a pulse waveform consisting of a rise time of 13 µs from 0 V to 30 V, a dwell width of 13 µs, a fall time of 38 µs from 30 V to -30 V, a dwell of 30 µs, and a final rise time of 13 µs to reach 0 V. The separation distance between the nozzle tip and the substrate surface was set at 0.4 mm. The nozzle temperature was maintained at 30 °C. The jetting driver was triggered by the camera. A high-speed camera (FASTCAM APX RS, Photron Europe Ltd.) in conjunction with a 20x magnification microscopic objective lens (M Plan, Nikon U.K. Ltd.) and a backlighting system (HPLS-30-02, Thorlabs Ltd.) were used to observe the droplet impact. By using 90,000 frames per second (fps), an image every 11 µs was obtained with the shutter speed set to 2 µs. In order to verify the droplet oscillation frequency, a faster frame rate of 180,000 fps was employed. Individual frames consisted of 128 x 96 pixels (128 x 32 at 180,000 fps) with 0.73 µm pixel size. Typical droplet impact speeds were measured to be in the range 0.8–1.2 m s^{-1}.

Atomic force microscopy (AFM) images were collected in tapping mode at 20 °C in ambient air (Nanoscope III, Digital Instruments Inc.). The stiff silicon cantilever had a spring constant of 42–83 N m^{-1} (Nanoprobe, Digital Instruments Inc.). Root-mean-square (RMS) roughness values were calculated over 50 μm x 50 μm scan areas.

Hardness values were obtained by microindentation (MVK-H2, Mitutoyo, Inc.) using a standard Vickers tip and a force of 20 mN (ASTM E384 - 11e1).[33] Elastic modulus values were determined by nanoindentation (Hysitron T1 950 Tribo-Indentor) using a Berkovich tip. The specimens were indented to a maximum depth of 50 nm using the indenter system set in a depth-control mode (10% of the sample thickness as per ISO 14577-4). The indentation procedure involved the following steps: (i) loading over 5 s to reach the maximum indentation depth, (ii) holding in this position for 2 s, and (iii) unloading over a period of 5 s. The hardness and Young's modulus were then calculated from the load-displacement data using the Oliver and Pharr method. 40 indents were made on each sample. The tip area function (contact area as a function of contact depth) was calibrated using a standard quartz sample; and then checked using single crystal aluminium to be within 5% of the manufacturer's specification.

3. RESULTS

3.1 Non-Crosslinked Versus Crosslinked Plasma Halogenated Polybutadiene

The XPS elemental composition of spin coated polybutadiene showed the presence of some oxygen content, which can be attributed to aerobic oxidation at the polymer film surface during the annealing step to remove trapped solvent, Table 1.[25] Following CF_4 and CCl_4 plasma halogenation, virtually all of this surface oxygen is lost accompanied with a high level of halogen incorporation. The slight increase in surface oxygen concentration following thermal crosslinking of these CF_4 and CCl_4 plasma halogenated films arises from the reaction between atmospheric oxygen and any unreacted polybutadiene alkene bonds located in the near-surface region.[34] In the absence of the polybutadiene layer, no film deposition was detected following either CF_4 or CCl_4 plasma exposure to silicon wafer surfaces; thereby confirming that plasma assisted surface halogenation rather than plasma deposition occurs for

polybutadiene.[35,36]

Table 1: XPS elemental compositions and static water contact angles for non-crosslinked and crosslinked: (a) untreated polybutadiene; (b) CF_4 plasma fluorinated polybutadiene; (c) CCl_4 plasma chlorinated polybutadiene; and (d) 20 nm thick ATRP poly(perfluorooctyl acrylate) brushes grown from (c). Polybutadiene film thickness = 1 μm.

		XPS Elemental Composition / ±0.5%				Static Contact Angle[†]	
		% C	% F	% Cl	% O	Microlitre / ±2°	Picolitre / ±5°
(a) Untreated polybutadiene	Non-Crosslinked	87.8	0.0	0.0	12.2	103	78
	Crosslinked	86.0	0.0	0.0	14.0	100	74
(b) CF_4 plasma fluorinated polybutadiene	Non-Crosslinked	40.9	57.1	0.0	2.0	134	106
	Crosslinked	41.0	54.6	0.0	4.4	133	105
(c) CCl_4 plasma chlorinated polybutadiene	Non-Crosslinked	56.5	0.0	43.5	0.0	88	74
	Crosslinked	55.3	0.0	43.0	1.7	85	72
(d) ATRP Poly($CF_3(CF_2)_5$ acrylate) brushes grown from (a)	Theoretical	40.7	48.2	3.7	7.4	–	–
	Non-Crosslinked	50.8	39.0	3.4	6.8	119	102
	Crosslinked	49.6	38.7	3.3	8.4	118	100

[†] In all cases, picolitre droplet (30 μm diameter) static contact angles are lower than for microlitre droplets (1.2 mm diameter) due to either the smaller droplet size relative to surface features,[37] or the high-speed impact of the picolitre droplets pushing the contact line beyond its equilibrium position.[38]

Infrared assignments for non-crosslinked polybutadiene are as follows:[25,39] $CH=CH_2$ stretch (3010 cm^{-1}), $-CH_2$ stretch (2922 cm^{-1}), $-CH_2$ symmetric stretch (2845 cm^{-1}), $-CH_2$ deformation (1438 cm^{-1}), -CH bending (967 cm^{-1}), and $CH=CH_2$ bending (913 cm^{-1}), Figure 3. No change in the infrared spectrum was observed following

plasmachemical halogenation, thereby indicating that only the outermost surface of the polybutadiene film is halogenated (i.e. limited to the XPS sampling depth of 2–5 nm).[25] Following thermal curing to crosslink these polybutadiene films, infrared analysis shows:[25] -OH stretch (3400 cm^{-1}), -CH$_2$ stretch (2922 cm^{-1}), aliphatic ester (1730 cm^{-1}), -CH$_2$ deformation (1438 cm^{-1}), and CH=CH$_2$ bending (913 cm^{-1}). The strong attenuation of the CH=CH$_2$ stretch (3010 cm^{-1}) confirms that bulk crosslinking has taken place, and the oxygenated species are attributable to aerial oxidation.[34]
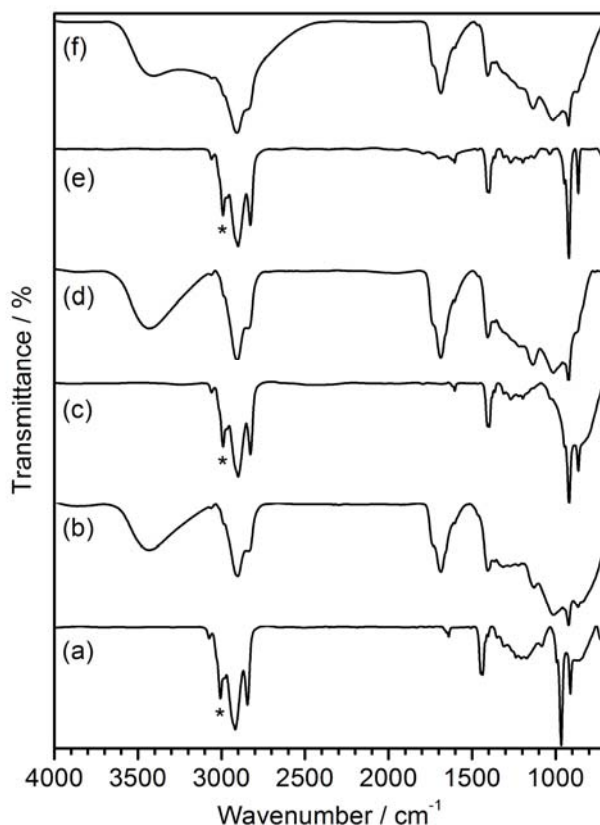

Figure 3: Infrared spectra of: (a) non-crosslinked polybutadiene; (b) crosslinked polybutadiene (c) non-crosslinked CF$_4$ plasma fluorinated polybutadiene; (d) crosslinked CF$_4$ plasma fluorinated polybutadiene; (e) non-crosslinked CCl$_4$ plasma chlorinated polybutadiene; and (f) crosslinked CCl$_4$ plasma chlorinated polybutadiene. * CH=CH$_2$ stretch (3010 cm^{-1}) for non-crosslinked polybutadiene.

In all cases, the AFM RMS surface roughness was measured to be less than 17 nm, which confirms the low level of plasmachemical roughening/texturing within the selected downstream plasma glow region due to the lack of surface bombardment by energetic electrical discharge species (e.g. ions),[28,29] Table 2.

Picolitre water droplet impact onto all of these surfaces displayed an initial spreading of the contact line to reach a maximum diameter. In the case of CF$_4$ plasma fluorinated polybutadiene, this was followed by dissipation of excess surface

free energy observed as oscillations of the droplet height (stemming from lower energy dissipation during spreading across a more hydrophobic surface), whilst motion of the contact line was inhibited due to pinning, Figure 4(a).[40] The droplet oscillation frequency subsequent to impact was measured by monitoring the change in height of the drop over time, Figure 4(b). In the case of untreated and CCl_4 plasma chlorinated polybutadiene, no droplet oscillations were observed due to the excess surface free energy being more efficiently dissipated during the initial droplet impact and spreading[41] (much lower contact angles, Table 1).
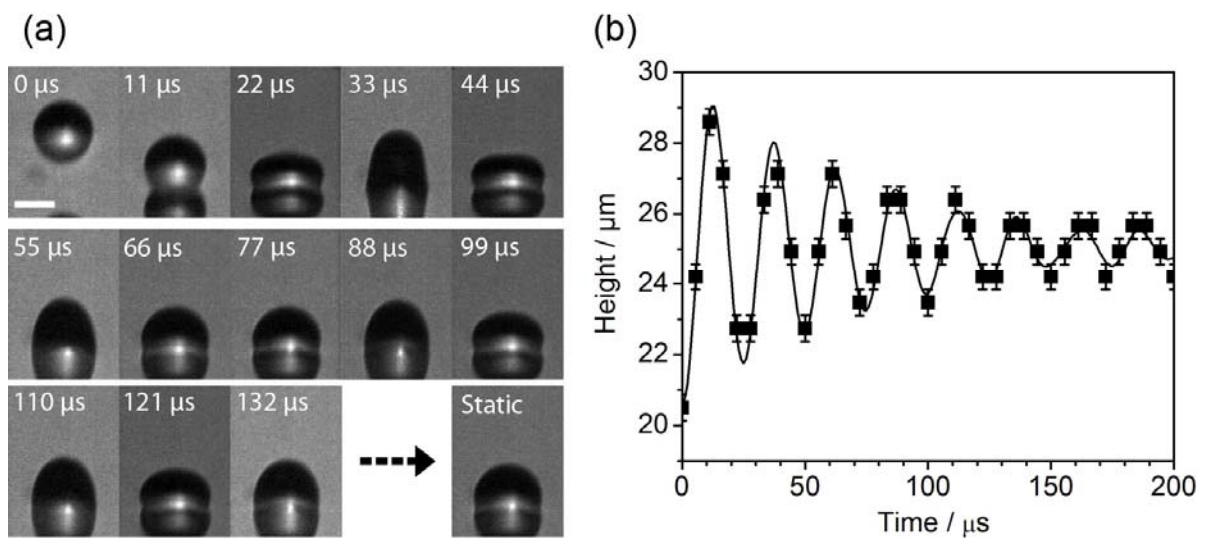

Figure 4: (a) High-speed video images (captured at 90,000 fps) of picolitre water droplet impact onto a hydrophobic CF_4 plasma fluorinated polybutadiene surface (reflection in substrate is seen in lower half, white scale bar = 20 μm); and (b) typical damped oscillation curve fitted to the experimental data for picolitre water droplet height fluctuation following impact. Oscillation frequencies were calculated from images captured at 180,000 fps.

The dynamics (oscillation frequency) of picolitre droplets following impact onto CF_4 plasma fluorinated polybutadiene were found to be dependent upon the film thickness, and film hardness (which could be altered by thermal crosslinking), Figure 5(a) and Table 2. A greater hardness reduces the influence of film thickness upon the change in oscillation frequency (despite the droplets retaining similar static water contact angles across the entire film thickness range), Table 1 and Figure 5(a). The approximately linear relationship between oscillation frequency and film thickness was found to breakdown beyond 500 nm, with the measured oscillation frequency for

the non-crosslinked and crosslinked CF_4 plasma fluorinated polybutadiene layers plateauing at 38.0 kHz and 33.6 kHz respectively.
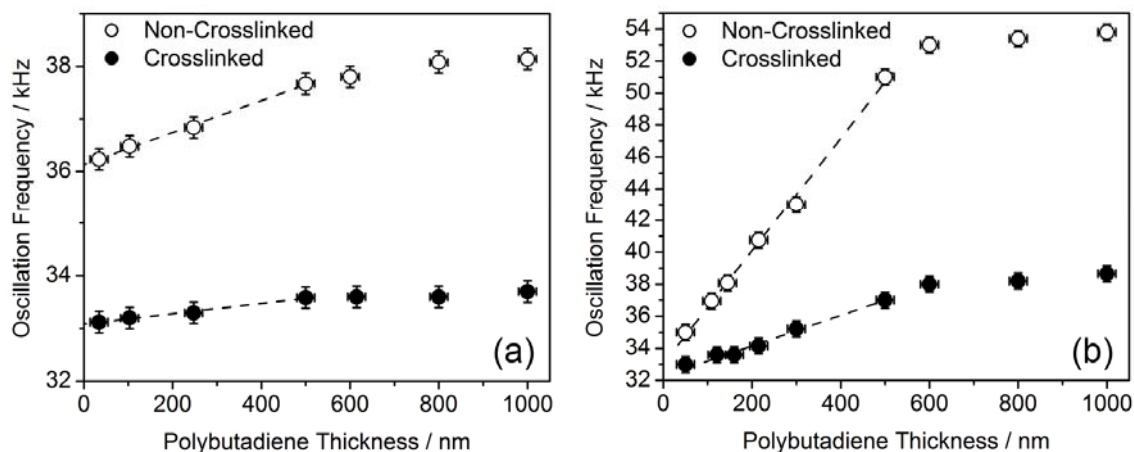

Figure 5: Oscillation frequencies of picolitre (30 µm diameter) water droplets following impact upon: (a) non-crosslinked and crosslinked CF_4 plasma fluorinated polybutadiene as a function of polybutadiene film thickness; and (b) 20 nm thick ATRP poly(perfluorooctyl acrylate) brushes grown from non-crosslinked and crosslinked CCl_4 plasma chlorinated polybutadiene as a function of polybutadiene film thickness. Microlitre and picolitre contact angles were not found to vary with film thickness, Table 1.

Nanoindentation was also carried out to determine the elastic modulus of the thin films, Table 2. The crosslinked polybutadiene films were found to have a higher elastic modulus compared to their non-crosslinked counterparts.

Table 2: AFM RMS roughness, microindentation hardness and nanoindentation elastic modulus of 1 µm thick films.

Layer	AFM RMS Roughness / nm	Microindentation Hardness / MPa	Nanoindentation Elastic Modulus / GPa
Non-crosslinked polybutadiene	7±1	17±2	1.2±0.03
Crosslinked polybutadiene	10±1	347±10	4.6±0.2
Non-crosslinked CF_4 plasma fluorinated polybutadiene	10±2	38±2	1.2±0.04
Crosslinked CF_4 plasma fluorinated polybutadiene	17±2	351±10	5.7±0.2
Non-crosslinked CCl_4 plasma chlorinated	6±1	21±2	1.2±0.09

polybutadiene			
Crosslinked CCl$_4$ plasma chlorinated polybutadiene	9±1	353±10	7.8±0.4

3.2 Perfluoroalkyl Polymer Brushes Surface Grafted From CCl$_4$ Plasma Chlorinated Polybutadiene ATRP Initiator Layers

Both non-crosslinked and crosslinked CCl$_4$ plasma chlorinated polybutadiene layers were utilised for the surface initiated ATRP growth of 20 nm thick poly(perfluorooctyl acrylate) polymer brushes with a view to further investigating the role of the subsurface thickness upon droplet impact dynamics. ATRP growth of the poly(perfluorooctyl acrylate) polymer brushes from the plasma chlorinated polybutadiene surfaces was confirmed by XPS and infrared analysis, Table 1 and Figure 6. Elemental XPS compositions were found to be consistent with the growth of poly(perfluorooctyl acrylate) brushes containing an end capping chlorine as part of the ATRP mechanism.[42] Infrared assignments for the perfluorooctyl acrylate monomer are as follows:[39] C=O stretching (1734 cm^{-1}), C=C stretching (1640 cm^{-1}), C=CH$_2$ in plane stretching (1412 cm^{-1}), -CF$_3$ stretching (1325 cm^{-1}), -CF$_2$-antisymmetric stretching (1242 cm^{-1}), and -CF$_2$- symmetric stretching (1145 cm^{-1}), Figure 6. Following surface ATRP grafting, the alkene bond features (C=C stretching (1640 cm^{-1}) and C=CH$_2$ in plane stretching (1412 cm^{-1})) have disappeared due to polymerisation having taken place.
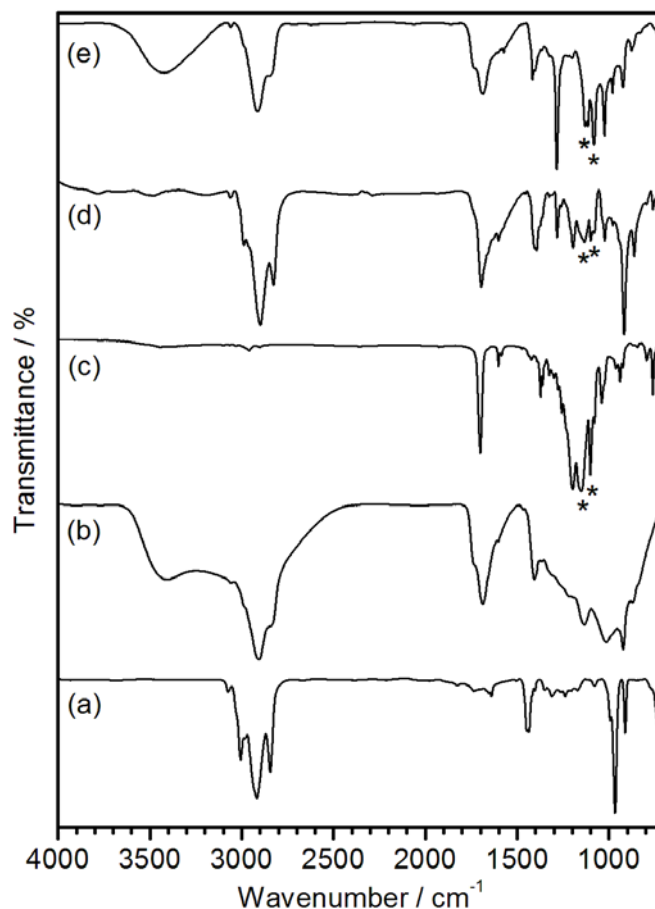
Figure 6: Infrared spectra of: (a) non-crosslinked CCl_4 plasma chlorinated polybutadiene; (b) crosslinked CCl_4 plasma chlorinated polybutadiene; (c) perfluorooctyl acrylate monomer; (d) 20 nm thick ATRP poly(perfluorooctyl acrylate) brushes grown from non-crosslinked CCl_4 plasma chlorinated polybutadiene; and (e) 20 nm thick ATRP poly(perfluorooctyl acrylate) brushes grown from crosslinked CCl_4 plasma chlorinated polybutadiene. * Perfluorooctyl acrylate CF_2 symmetric (1145 cm^{-1}) and antisymmetric (1242 cm^{-1}) stretching peaks.

Droplet oscillation frequencies following impact upon 20 nm thick ATRP poly(perfluorooctyl acrylate) brush layers grown from non-crosslinked and crosslinked CCl_4 plasma chlorinated polybutadiene were found to be governed by both the thickness and hardness of the underlying CCl_4 plasma chlorinated polybutadiene initiator layer, Table 2 and Figure 5(b). This was in conjunction with the picolitre droplet static contact angle remaining constant (around 100°) for both the non-crosslinked and crosslinked underlayer across the entire thickness range, Table 1. The approximately linear relationship between the underlayer thickness and oscillation frequency was found to breakdown for both the non-crosslinked and crosslinked CCl_4 plasma chlorinated polybutadiene underlayer beyond 500 nm, with the measured oscillation frequency plateauing at 53.8 kHz and 38.2 kHz respectively. Control experiments showed that water droplets impacting upon CCl_4

plasma chlorinated polybutadiene in the absence of the ATRP poly(perfluorooctyl acrylate) brush layer gave rise to spreading with no measurable oscillatory behaviour.

Because of their size, the picolitre droplets (30 μm diameter) evaporated within several seconds after impact. The surfaces were analysed by atomic force microscopy (AFM) several hours later, long after the droplets had dried. For all samples, approximately 30 μm diameter rings were observed, which are consistent with the formation of a wetting ridge, Figure 7. The ridge height significantly exceeds the 20 nm thickness of the ATRP poly(perfluorooctyl acrylate) brush, thereby indicative of subsurface deformation. The extent of lateral and vertical surface deformation during droplet impact was found to depend upon the thickness and hardness of the underlying CCl_4 plasma chlorinated polybutadiene ATRP initiator layer. Water droplet impact upon 20 nm thick ATRP poly(perfluorooctyl acrylate) brush layers grown from crosslinked (harder) CCl_4 plasma chlorinated polybutadiene exhibited a wetting ridge that was smaller in height and width compared to that measured following droplet impact onto ATRP poly(perfluorooctyl acrylate) brush layers grown from non-crosslinked (softer) CCl_4 plasma chlorinated polybutadiene of the same thickness, Figure 7. The ridge height of the surface deformation following droplet impact increased in a linear fashion as a function of underlayer thicknesses up to 500 nm, Figure 7(d). For underlayer thicknesses exceeding 500 nm, the deformation ridge height levelled off to 130–140 nm for non-crosslinked and 50–55 nm for crosslinked CCl_4 plasma chlorinated polybutadiene underlayer (which is consistent with the aforementioned plateauing of oscillation frequency beyond 500 nm polybutadiene film thickness).
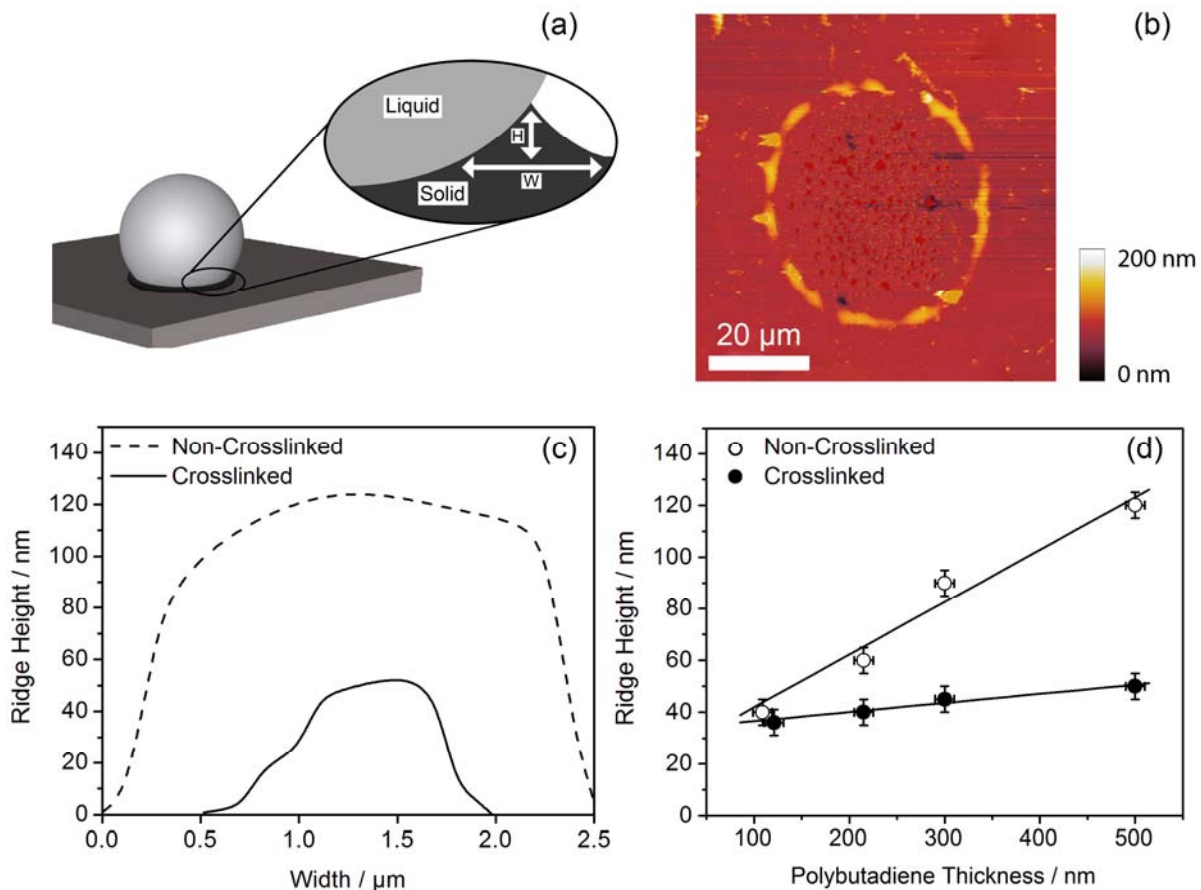
Figure 7: (a) Schematic of surface deformation induced by a droplet impacting onto a soft surface; (b) AFM height image of surface after single 30 μm diameter picolitre water droplet impact upon 20 nm thick ATRP poly(perfluorooctyl acrylate) brushes grown from 500 nm thick non-crosslinked CCl_4 plasma chlorinated polybutadiene; (c) height and width of wetting ridge following 30 μm diameter picolitre droplet impact upon poly(perfluorooctyl acrylate) brushes grown from 500 nm thick non-crosslinked and crosslinked CCl_4 plasma chlorinated polybutadiene; and (d) ridge height of surface deformation as a function of CCl_4 plasma chlorinated polybutadiene underlayer thickness for 20 nm thick ATRP poly(perfluorooctyl acrylate) brushes (note that for underlayer thicknesses exceeding 500 nm, the deformation ridge height levelled off to 130–140 nm for non-crosslinked and 50–55 nm for crosslinked CCl_4 plasma chlorinated polybutadiene underlayer).

4. DISCUSSION

Picolitre droplet impact has been studied for a range of hydrophobic surfaces with variable underlayer hardness. CF_4 plasma fluorinated polybutadiene provides a hydrophobic surface which can be crosslinked to alter its mechanical properties, Table 2.[25] Picolitre droplet impact onto these hydrophobic surfaces results in oscillation of the droplet height about a final static value, caused by excess energy not being fully dissipated through spreading. Unlike previous studies on rougher,

superhydrophobic surfaces,[30,38] the contact line remains pinned during the majority of the oscillation cycle, with only a small retraction evidenced after the initial spreading, Figure 4. The oscillation frequency of droplets after impact onto these surfaces was found to depend upon the polybutadiene layer hardness and thickness. The observed rise in oscillation frequency with increasing polymer film thickness is greater for soft (non-crosslinked) CF_4 plasma fluorinated polybutadiene compared to its harder (crosslinked) counterpart, Figure 5(a).

A similar trend is observed for ATRP hydrophobic poly(perfluoroalkyl acrylate) polymer brushes grown onto CCl_4 plasma chlorinated polybutadiene (non-crosslinked verus crosslinked) initiator surfaces. For the same 20 nm increase in thickness attributable to poly(perfluorooctyl acrylate) ATRP polymer brush growth (constant contact angle), the picolitre droplet impact dynamics are found to be governed by the underlayer hardness and exhibit a thickness dependence. The oscillation frequency is measured to be higher for the softer (non-crosslinked) polybutadiene underlayer compared to its harder (crosslinked) analogue at similar film thickness, Figure 5(b) and Table 2. Given that the ridge height of the surface deformation following droplet impact significantly exceeds the 20 nm increase in thickness attributable to the ATRP poly(perfluorooctyl acrylate) brush layer, this can be taken as being indicative of subsurface deformation.

The thin polymer film undergoes both elastic and plastic deformation at the contact line. The extent of elastic deformation is given by:[43]

$$\zeta \propto \frac{\gamma \sin \theta}{G}$$
Equation 1

where ζ is the vertical displacement, γ is the liquid/vapour interfacial tension, θ is the equilibrium contact angle of the droplet, and G is the elastic shear modulus of the solid. The measured values of the Young's modulus (Table 2) lie in the range of 1–8 GPa, which is much higher than typical values for elastomers (~ MPa)[44] suggesting that partial cross-linking may have occurred during the vacuum annealing step. For an elastomer, the shear modulus is approximately one third of the Young's modulus and consequently the elastic deformation from Equation 1 are in the range of 0.3–2 Å. These values are very much less than the thickness of the polymer films

and it therefore seems unlikely that elastic deformation contributes to the observed dependence of the oscillation frequency on the thickness of the polymer layer.

The occurrence of plastic deformation is evidenced by the observation of a persistent wetting ridge in AFM after the droplet has dried, Figure 7. The local stress at the contact line, assuming it acts over an interfacial width of the order of 0.5 nm, is $\sim 10^8$ Pa which exceeds the measured (compressive) hardness of the non-crosslinked polybutadiene films and is approaching the hardness of the cross-linked films, Table 2. It is therefore unsurprising that the films yield under the tensile stress at the contact line. The height of the wetting ridge was observed to increase with the underlayer polybutadiene film thickness and to decrease with the hardness of the film, Figure 7(d). The wetting ridge has a negligible effect on the static contact angles of picolitre droplets, which are found to remain constant within error across a wide range of underlayer thicknesses. However, the size of this ridge does affect the droplet dynamics. The observed rise in droplet oscillation frequency following impact with increasing film thickness for all of the surfaces investigated correlates to greater surface deformation (ridge height) for thicker films,[23,45,46,47] Figure 7. Some interpenetration of the ATRP poly(perfluorooctyl acrylate) brushes into the CCl_4 plasma chlorinated polybutadiene initiator underlayer might also be contributing towards the observed plastic deformation during droplet impact.

In all cases, the oscillation frequency and extent of surface deformation reached a plateau above 500 nm underlayer thicknesses, regardless of the contact angle of the droplet or the mechanical properties of the film, Figure 5. The oscillation frequency thus appears to be correlated with the extent of plastic deformation, though the physical reason for this relationship remains unclear.

Such picolitre droplet impact dynamics onto soft surfaces are of relevance to microfluidics and inkjet printing (dried ink feature size and homogeneity).[48] Furthermore, they provide a direct means to probe the mechanical properties of functional nanofilms.[49]

5. CONCLUSIONS

The dynamics of picolitre water droplets following impact onto ultra thin films is governed by the underlayer film thickness and mechanical hardness. Thicker and

softer films give rise to higher oscillation frequencies due to greater surface deformation (ridge formation) around the contact line.

6. ACKNOWLEDGEMENTS

7. REFERENCES

[1]   Gervais, T.; El-Ali, J.; Günther, A.; Jensen, K. F. Flow-Induced Deformation of Shallow Microfluidic Channels. *Lab Chip* **2006**, *6*, 500–507.

[2]   Pu, G.; Ai, J.; Severtson, S. J. Drop Behavior on a Thermally-Stripped Acrylic Polymer: Influence of Surface Tension Induced Wetting Ridge Formation on Retention and Running. *Langmuir* **2010**, *26*, 12696–12702.

[3]   Li, C.; Jiang, H. Electrowetting-Driven Variable-Focus Microlens on Flexible Surfaces. *Appl. Phys. Lett.* **2012**, *100*, 231105.

[4]   Sokuler, M.; Auernhammer, G. K.; Roth, M.; Liu, C.; Bonacurrso, E.; Butt, H.-J. The Softer the Better: Fast Condensation on Soft Surfaces. *Langmuir* **2010**, *26*, 1544–1547.

[5]   Sirringhaus, H.; Kawase, T.; Friend, R. H.; Shimoda, T.; Inbasekaran, M.; Wu, W.; Woo, E. P. High-Resolution Inkjet Printing of All-Polymer Transistor Circuits. *Science* **2000**, *290*, 2123–2126.

[6]   Wang, J. Z.; Zheng, Z. H.; Li, H. W.; Huck, W. T. S.; Sirringhaus, H. Dewetting of Conducting Polymer Inkjet Droplets on Patterned Surfaces. *Nat. Mater.* **2004**, *3*, 171–176.

[7]   Sele, C. W.; von Werne, T.; Friend, R. H.; Sirringhaus, H. Lithography-Free, Self-Aligned Inkjet Printing with Sub-Hundred-Nanometer Resolution. *Adv. Mater.* **2005**, *17*, 997–1001.

[8]   Doggart, J.; Wu, Y.; Liu, P.; Zhu, S. Facile Inkjet-Printing Self-Aligned Electrodes for Organic Thin-Film Transistor Arrays with Small and Uniform Channel Length. *ACS Appl. Mater. Interfaces* **2010**, *2*, 2189–2192.

[9]   Barbulovic-Nad, I.; Lucente, M.; Sun, Y.; Zhang, M.; Wheeler, A. R.; Bussmann, M. Bio-Microarray Fabrication Techniques—A Review. *Crit. Rev. Biotechnol.* **2006**, *26*, 237–259.

[10] Tan, C. P.; Cipriany, R.; Lin, D. M.; Craighead, H. G. Nanoscale Resolution, Multicomponent Biomolecular Arrays Generated By Aligned Printing With Parylene Peel-Off. *Nano Lett.* **2010**, *10*, 719–725.

[11] Arrabito, G.; Pignataro, B. Inkjet Printing Methodologies for Drug Screening. *Anal. Chem.* **2010**, *82*, 3104–3107.

[12] Mironov, V.; Boland, T.; Trusk, T.; Forgacs, G.; Markwald, R. R. Organ Printing: Computer-Aided Jet-Based 3D Tissue Engineering. *Trends Biotechnol.* **2003**, *21*, 157–161.

[13] Xu, T.; Jin, J.; Gregory, C.; Hickman, J. J.; Boland, T. Inkjet Printing of Viable Mammalian Cells. *Biomaterials* **2005**, *26*, 93–99.

[14] Bharathan, J.; Yang, Y. Polymer Electroluminescent Devices Processed by Inkjet Printing: I. Polymer Light-Emitting Logo. *Appl. Phys. Lett.* **1998**, *72*, 2660–2662.

[15] Chang, S.-C.; Bharathan, J.; Yang, Y.; Helgeson, R.; Wudl, F.; Ramey, M. B.; Reynolds, J. R. Dual-Color Polymer Light-Emitting Pixels Processed by Hybrid Inkjet Printing. *Appl. Phys. Lett.* **1998**, *73*, 2561–2563.

[16] Shanahan, M. E. R. The Influence of Solid Micro-Deformation on Contact Angle Equilibrium. *J. Phys. D: Appl. Phys.* **1987**, *20*, 945–950.

[17] Shanahan, M. E. R. The Spreading Dynamics of a Liquid Drop on a Viscoelastic Solid. *J. Phys. D: Appl. Phys.* **1988**, *21*, 981–985.

[18] Extrand, C. W.; Kumagai, Y. Contact Angles and Hysteresis on Soft Surfaces. *J. Colloid Interface Sci.* **1996**, *184*, 191–200.

[19] White, L. R. The contact angle on an elastic substrate. 1. The Role of Disjoining Pressure in the Surface Mechanics. *J. Colloid Interface Sci.* **2003**, *258*, 82–96.

[20] Pericet-Cámara, R.; Best, A.; Butt, H.-J.; Bonaccurso, E. Effect of Capillary Pressure and Surface Tension on the Deformation of Elastic Surfaces by Sessile Liquid Microdrops: An Experimental Investigation. *Langmuir* **2008**, *24*, 10565–10568.

[21] Pericet-Camara, R.; Auernhammer, G. K.; Koynov, K.; Lorenzoni, S.; Raiteri, R.; Bonaccurso, E. Solid-Supported Thin Elastomer Films Deformed by Microdrops. *Soft Matter* **2009**, *5*, 3611–3617.

[22] Shanahan, M. E. R.; Carré, A. Viscoelastic Dissipation in Wetting and Adhesion Phenomena. *Langmuir* **1995**, *11*, 1396–1402.

[23] Pu, G.; Severtson, S. J. Dependence of Wetting Behavior on the Thickness of Highly Viscoelastic Films. *J. Phys. Chem. C* **2011**, *115*, 18729–18735.

[24] Rioboo, R.; Voué, M.; Adão, Conti, J.; Vaillant, A.; Seveno, D.; De Coninck, J. Drop Impact on Soft Surfaces: Beyond the Static Contact Angles. *Langmuir* **2010**, *26*, 4873–4879.

[25] Woodward, I.; Schofield, W. C. E.; Roucoules, V.; Badyal, J. P. S. Super-Hydrophobic Surfaces Produced by Plasma Fluorination of Polybutadiene Films. *Langmuir* **2003**, *19*, 3432–3438.

[26] Wang, J.-S.; Matyjaszewski, K. Controlled/"Living" Radical Polymerization. Atom Transfer Radical Polymerization in the Presence of Transition-Metal Complexes. *J. Am. Chem. Soc.* **1995**, *117*, 5614–5615.

[27] Granville, A. M.; Brittain, W. J. Stimuli-Responsive Semi-Fluorinated Polymer Brushes on Porous Silica Substrates. *Macromol. Rapid Commun.* **2004**, *25*, 1298–1302.

[28] Harshbarger, W. R.; Porter, R. A.; Miller, T. A.; Norton, P. A Study of the Optical Emission From an RF Plasma During Semiconductor Etching. *Appl. Spectrosc.* **1977**, *31*, 201–207.

[29] Grill, V.; Walder, G.; Scheier, P.; Kurdel, M.; Märk, T. D. Absolute Partial and Total Electron Impact Ionization Cross Sections for C_2H_6 from Threshold up to 950 eV. *Int. J. Mass Spectrom. Ion Processes* **1993**, *129*, 31–42.

[30] Brown, P. S.; Talbot, E. L.; Wood, T. J.; Bain, C. D.; Badyal, J. P. S. Superhydrophobic Hierarchical Honeycomb Surfaces. *Langmuir* **2012**, *28*, 13712–13719.

[31] Evans, J. F.; Gibson, J. H.; Moulder, J. F.; Hammond, J. S.; Goretzki, H. Angle Resolved ESCA Analysis of Plasma Modified Polysterene. *Fresenius J. Anal. Chem.* **1984**, *319*, 841–844.

[32] Tabet, M. F.; McGahan, W. A. Use of Artificial Neural Networks to Predict Thickness and Optical Constants of Thin Films from Reflectance Data. *Thin Solid Films* **2000**, *370*, 122–127.

[33] ASTM Standard E384 - 11e1, " Standard Test Method for Knoop and Vickers Hardness of Materials," ASTM International, West Conshohocken, PA, 2011, DOI: 10.1520/E0384-11E01, www.astm.org (accessed Jul. 29 2013).

[34] Raghavan, D.; Gu, X.; Nguyen, T.; VanLandingham, M.; Karim, A. Mapping Polymer Heterogeneity Using Atomic Force Microscopy Phase Imaging and Nanoscale Indentation. *Macromolecules* **2000**, *33*, 2573–2583.

[35] Strobel, M.; Corn, S.; Lyons, C. S.; Korba, G. A. Plasma fluorination of polyolefins. *J. Polym. Sci. Part A: Polym. Chem.* **1987**, *25*, 1295.

[36] Inagaki, N.; Tasaka, S.; Imai, M. Hydrophilic Surface Modification of Polypropylene Films by CCl_4 plasma. *J. Appl. Polym. Sci.* **1993**, *48*, 1963–1972.

[37] Good, R. J.; Koo, M. N. The Effect of Drop Size on Contact Angle. *J. Colloid Inter. Sci.* **1979**, *71*, 283–292.

[38] Brown, P. S.; Berson, A.; Talbot, E. L.; Wood, T. J.; Schofield, W. C. E.; Bain, C. D.; Badyal, J. P. S. Impact of Picoliter Droplets on Superhydrophobic Surfaces with Ultralow Spreading Ratios. *Langmuir* **2011**, *27*, 13897–13903.

[39] Lin-Vien, D.; Colthrup, N. B.; Fateley, W. G.; Grasselli, J. G. *The Handbook of Infrared and Raman Characteristic Frequencies of Organic Molecules*; Academic Press, Inc.: San Diego, 1991.

[40] Gao, L.; McCarthy, T. J. Contact Angle Hysteresis Explained. *Langmuir* **2006**, *22*, 6234–6237.

[41] Mao, T.; Kuhn, D. C. S.; Tran, H. Spread and Rebound of Liquid Droplets Upon Impact on Flat Surfaces. *AIChE J.* **1997**, *43*, 2169–2179.

[42] Zhang, H.; Schubert, U. S. Iron Halide Mediated Atom Transfer Radical Polymerization of Methyl Methacrylate with N-alkyl-2-pyridylmethanimine as the Ligand. *J. Polym. Sci., Part A: Polym. Chem.* **2004**, *42*, 4882–4894.

[43] Shanahan, M. E. R.; Carré, A. *Colloids Surf., A* Spreading and Dynamics of Liquid Drops Involving Nanometric Deformations on Soft Substrates. *Colloids Surf., A* **2002**, *206*, 115–123.

[44] Textbook of Polymer Science, 3rd Ed., Billmeyer, F. W. Jr.: Wiley, New York, 1984.

[45] Voué, M.; Rioboo, R.; Bauthier, C.; Conti, J.; Charlot, M.; De Coninck, J. Dissipation and Moving Contact Lines on Non-Rigid Substrates. *J. Eur. Ceram. Soc.* **2003**, *23*, 2769–2775.

[46] Yu, Y.-S.; Yang, Z.; Zhao, Y.-P. Role of Vertical Component of Surface Tension of the Droplet on the Elastic Deformation of PDMS Membrane. *J. Adhes. Sci. Technol.* **2008**, *22*, 687–698.

[47] Yu, Y.-S.; Zhao, Y.-P. Elastic deformation of soft membrane with finite thickness induced by a sessile liquid droplet. *J. Colloid. Interface. Sci.* **2009**, *339*, 489–494.

[48] Calvert, P. Inkjet Printing for Materials and Devices. *Chem. Mater.* **2001**, *13*, 3299–3305.

[49] Long, D.; Ajdari, A.; Leibler, L. Static and Dynamic Wetting Properties of Thin Rubber Films. *Langmuir* **1996**, *12*, 5221–5230.